

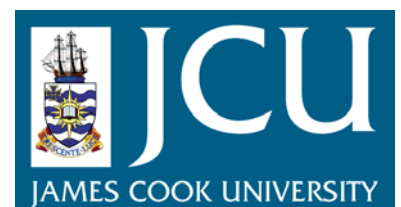
JCU ePrints

This file is part of the following reference:

Marshall, Lucas (2003) *Brecciation within the Mary Kathleen Group of the Eastern Succession, Mt Isa Block, Australia: Implications of district-scale structural and metasomatic processes for Fe-oxide-Cu-Au mineralisation*. PhD thesis, James Cook University.

Access to this file is available from:

<http://eprints.jcu.edu.au/8243>



**Brecciation within the Mary Kathleen Group of the
Eastern Succession, Mt Isa Block, Australia: Implications
of district-scale structural and metasomatic processes for
Fe-oxide-Cu-Au mineralisation**

Thesis submitted by
Lucas John Marshall, B.Sc. (Hons.) (UBC)
in May, 2003,

for the degree of Doctor of Philosophy in
the School of Earth Sciences
at James Cook University of North Queensland

STATEMENT OF ACCESS

I, the undersigned author of this work, understand that James Cook University will make this thesis available for use within the University Library and, via the Australian Digital Theses network, for use elsewhere.

I understand that, as an unpublished work, a thesis has significant protection under the Copyright Act and;

I do not wish to place any further restriction on access to this work

Or

I wish this work to be embargoed until

Or

I wish the following restrictions to be placed on this work:

Signature

Date

ELECTRONIC COPY

I, the undersigned, the author of this work, declare that the electronic copy of this thesis provided to the James Cook University Library, is an accurate copy of the print thesis submitted, within the limits of the technology available.

Signature

Date

STATEMENT ON SOURCES

Declaration

I declare that this thesis is my own work and has not been submitted in any form for another degree or diploma at any university or other institution of tertiary education. Information derived from the published or unpublished work of others has been acknowledged in the text and a list of references is given.

.....
(Signature)

.....
(Date)

ABSTRACT

The Eastern Succession of the Proterozoic Mt Isa Block, including the Cloncurry District and the Mary Kathleen Fold Belt (MKFB), contains numerous examples of Fe-oxide-Cu-Au mineralisation. Most deposits, including Ernest Henry, Eloise, Starra and Mt Elliott formed after the peak of ca. 1600-1575 Ma upper greenschist to amphibolite facies metamorphism, and during the waning phases of the Isan Orogeny. Mineralisation was broadly synchronous with emplacement of voluminous phases of the Williams and Narku batholiths (ca. 1550 – 1500 Ma) and widespread brecciation and accompanying metasomatism. Brecciation and metasomatism were best developed within Cover Sequence 2 stratigraphy, and in particular within calc-silicate rock and meta-siltstone stratigraphy of the Corella Formation, the predominant rocks of the Mary Kathleen Group.

The geometry and distribution of brecciation in the Corella Formation was in part controlled by retrograde buckle folding imposed on a heterogeneous rock sequence that was fractured and boudinaged both pre- and syn-buckle folding. Brecciation is far more widespread in the Cloncurry District relative to the MKFB, reflecting in part a larger proportion of stratigraphy in the Cloncurry District that was at low angles to the shortening direction during the waning phases of the Isan Orogeny, favoring refolding and consequent fracturing. Variations in regional structural trends reflect strain partitioning around competent intrusive bodies, fault reactivation and refolding. Other contributing factors for brecciation include low temperature conditions during late deformation, and the proximity to voluminous intrusions, the emplacement of which likely resulted in transient elevated fluid pressure and strain rates, favoring fracturing and brecciation. The relative paucity of brecciation in most stratigraphic units outside of the Corella Formation reflects a high proportion of incompetent stratigraphy in these sequences (e.g. voluminous micaceous schists within the Soldiers Cap Group), which were able to accommodate strain by plastic flow.

The broad-scale geometry of the Cloncurry District reflects Cover Sequence 3 rocks overlying Cover Sequence 2 rocks, the two sequences being separated by early faults. Marbles within the Corella Formation, and schists in other stratigraphic sequences were not prone to brittle failure, and acted as low permeability barriers to fluid flow. These horizons allowed for the attainment of elevated fluid pressures within large volumes of brecciated rock. During the final stages of brecciation, these low competence marbles and schists were fractured and brecciated, predominantly within discrete fault zones. This shift from widespread brittle-ductile to purely brittle deformation likely reflects progressive cooling, as well as locally elevated fluid pressure and/or strain rate associated with pluton emplacement and degassing. A synchronous district-scale shift from compression to transtension facilitated the development of vertically continuous zones of dilation within faults, resulting in very large fluid pressure gradients and catastrophic fault valving.

Brecciation was accompanied by widespread metasomatism that ranges from high temperature (400° - 600°C) Na-(Ca)-rich assemblages (e.g. albite ± actinolite, clinopyroxene, scapolite, magnetite, titanite, etc.) to retrograde (<400°C) chloritic assemblages. Interpretation of stable (O and C) and radiogenic (Sr) isotopes and mineral chemistry is consistent with this spectrum of alteration assemblages reflecting metasomatic fluids of two predominant origins. The oxygen and carbon isotopic signature of carbonates from Na-(Ca) assemblages indicates that fluids responsible for this style of alteration were not simply equilibrated with magmatic rocks, but were exsolved from crystallizing plutons. Low temperature, low salinity fluids of inferred meteoric origin were introduced late in the paragenesis, and do not appear to have contributed significantly to the mass budgets of Cu-Au ore systems in the district.

Extensive fluid-wallrock interaction prior to mineralisation appears to have been important in the genesis of some deposits that record K- and Fe-rich alteration haloes, including for example the Ernest Henry deposit. However, the occurrence of

skarn-like, intrusion-proximal mineralisation that lacks significant K- and Fe-enrichment at for example Mt Elliott, indicates that fluid-wallrock interaction was not a necessary precursor for all styles of Cu-Au mineralisation in the Cloncurry District.

ACKNOWLEDGEMENTS

I would like to thank Nick Oliver for initiating this project, and for his enthusiasm and support throughout. Funding from JCU, the pmd*CRC and the Society of Economic Geologists are all gratefully acknowledged. MIM Exploration provided logistical support in the field, and Ernest Henry Mining arranged access to drill core at the Ernest Henry deposit. Brian Curtisse is thanked for hospitality at Roxmere station, and Mick Carew, Wade Hodgson, Ha Sy, Bin Fu, Geordie Mark, John McLellan, and Han Long Ying are all acknowledged as jovial field companions. Pete and SheepDog provided the entertainment in Cloncurry, while that task was left up to Red and the late Wally at Roxmere station.

MIM Exploration allowed access to geophysical data, including wavelet-processed data from Fractal Graphics. Barry Murphy, Paul Gow and Peter Jones are all thanked for assistance in manipulating and interpreting the geophysical data. Many thanks to the people and institutions that supplied or assisted with analytical data, including: Ian Cartwright and Ben Petrides (Monash University) for carbon and oxygen isotope analyses; Zach Sharp (University of New Mexico) for oxygen isotope analyses; David Bruce (University of Adelaide) for strontium isotope analyses; Hans Machel and Jeff Lonnee (University of Alberta) for access to, and assistance with CL equipment; Kevin Blake and Alan Chapel (James Cook University) for assistance with microprobe and GADDS analyses; Norm Pearson (Macquarie University) for assistance with LA-ICPMS analysis.

Aspects of this thesis have benefited significantly from discussion with Mike Roberts, Graham Shields, James Cleverley, Bin Fu, Tim Baker, Mike Rubenach, Pat Williams, Peter Pollard, Roger Taylor, Dan Mollicone, Garry Davidson, Geordie Mark, Damien Foster, Tom Blenkinsop, Mick Carew, Josh Bryant, Chris Salt, Dan Johnson, Owen Hatton, Kathryn Lewthwaite and many others. Tom Blenkinsop, Rick Sibson, Rod Holcombe, Mike Roberts and Julian Stephens are all thanked for their time and attention in reading drafts of various manuscripts. Finally, I can't thank Ha Sy enough for her support, humor and in general for toughing it in the tropics.

TABLE OF CONTENTS

TITLE PAGE	i
STATEMENT OF ACCESS	ii
ABSTRACT	iii
ACKNOWLEDGEMENTS	vi
TABLE OF CONTENTS	vii
LIST OF FIGURES	xiii
LIST OF TABLES	xxi
DECLARATION	xxii
CHAPTER 1:	1
INTRODUCTION AND REGIONAL GEOLOGY	
1.1 INTRODUCTION	2
1.2 THESIS AIMS	6
1.3 RESEARCH TOOLS AND METHODOLOGY	7
1.3.1 Field mapping, core logging and hand specimens	7
1.3.2 Structural interpretation	8
1.3.3 Analytical samples	8
1.3.4 Mineral chemistry	8
1.3.5 Isotopes	9
1.4 THESIS STRUCTURE	9
1.5 PREVIOUS RESEARCH	12
1.5.1 Tectonostratigraphic zones within the Mt Isa Block	12
1.5.2 Tectonostratigraphic sequences of the Eastern Succession	13
1.5.3 Structural history	17
1.5.4 Metamorphic history	20
1.5.5 Absolute timing of deformation and metamorphism	20
1.5.6 Intrusive events	23
1.5.7 Brecciation	25
1.5.8 Metasomatism	27
1.5.9 Mineralisation	28
CHAPTER 2:	31
COMPLEXITIES IN THE REGIONAL STRUCTURAL GEOMETRY OF THE EASTERN SUCCESSION, MT ISA BLOCK, AUSTRALIA	
2.1 INTRODUCTION	32
2.1.1 Previous work	32
2.1.2 Approach and methodology	36

2.2	STRUCTURAL OBSERVATIONS	38
2.2.1	Regional structural patterns	38
2.2.2	Budenberri area	39
2.2.3	Mary Kathleen Fold Belt: Tribulation and Mt Philp areas	39
2.2.4	Cloncurry Region	39
2.2.5	Superposed fold analysis	44
2.2.6	Late fault architecture	48
2.2.7	Cloncurry 3D architecture	51
2.3	DISCUSSION	57
2.3.1	D ₁ : Thrusting and folding	57
2.3.2	D ₂ : E-W shortening and isoclinal folding	58
2.3.3	Reorientation of D ₂ folds	60
2.3.4	D ₃ : E-W shortening, heterogeneous folding, reverse and wrench faulting	61
2.4	CONCLUSIONS	63
CHAPTER 3:		65
VOLUME GAIN FOLDING AND EFFECTIVE LAYER THINNING AS MODIFICATIONS ON MODELS OF TANGENTIAL LONGITUDINAL STRAIN		
3.1	INTRODUCTION	66
3.2	REVIEW OF FOLDING MECHANISMS	67
3.2.1	Tangential Longitudinal Strain	69
3.3	VARIATIONS ON MODELS FOR TLS	71
3.3.1	Volume gain folding	71
3.3.2	Effective layer thinning	73
3.4	DISCUSSION	75
3.5	CONCLUSIONS	75

CHAPTER 4:	77
CONTROL OF BUCKLE FOLDING AND THE LOCAL STRESS FIELD ON THE DISTRIBUTION OF WIDESPREAD BRECCIATION IN THE CLONCURRY DISTRICT, MT ISA BLOCK, AUSTRALIA	
4.1 INTRODUCTION	78
4.1.1 Terminology and classification schemes	81
4.1.2 Buckle folds and accommodation structures	85
4.1.3 Cloncurry District Geology	85
4.2 CLONCURRY DISTRICT STRUCTURAL OBSERVATIONS	86
4.2.1 D2: Soldiers Cap Group	86
4.2.2 D3: Soldiers Cap Group	88
4.2.3 D2: Corella Formation	88
4.2.4 D3: Corella Formation	91
4.3 FOLDS, FRACTURES, BOUDINS AND BRECCIAS	94
4.3.1 Folded boudin trains and boudin rotation	94
4.3.2 Brecciated multilayers	96
4.3.3 Accommodation structures	99
4.4 DISCUSSION	99
4.4.1 Brecciation as an accommodation mechanism	101
4.4.2 Contributing factors for brecciation in the Corella Formation	105
4.4.3 Implications for metasomatic fluid pathways	107
4.5 CONCLUSIONS	107
APPENDIX 4.A: CALCULATIONS FOR FIGURE 4.15	109
CHAPTER 5:	114
EXAMPLES OF DILATIONAL FAULT ZONE BRECCIATION AND VEINING IN THE EASTERN SUCCESSION, MT ISA BLOCK, AND DISCUSSION OF POTENTIAL GENETIC MECHANISMS	
5.1 INTRODUCTION	115
5.1.1 Dilational fault zones and brecciation	117
5.1.2 Regional geology	119

5.2	FIELD EXAMPLES OF DILATIONAL FAULT ZONES	121
5.2.1	Mt Elliott Cu-Au	121
5.2.2	Roxmere-Marimo shear zone	123
5.2.3	Tribulation calcite vein	126
5.2.4	Gilded Rose breccia type area	131
5.2.5	Ernest Henry Cu-Au	133
5.3	DISCUSSION	138
5.3.1	Clast generation and implosion brecciation	138
5.3.2	Large width veining	141
5.3.3	Clast transport, fluidization and gas streaming	145
5.3.4	Catastrophic fault valving	151
5.4	CONCLUSIONS	152

CHAPTER 6: 154
SILICATE AND OXIDE MINERAL AND ISOTOPE GEOCHEMISTRY AS
MONITORS OF FLUID CHEMISTRY IN DISTRICT-SCALE
METASOMATIC PROCESSES, EASTERN SUCCESSION, MT ISA BLOCK

6.1	INTRODUCTION	155
6.1.1	Regional geology	156
6.2	METASOMATIC ASSEMBLAGES	159
6.2.1	Roxmere – Marimo area	159
6.2.2	Budenberri	167
6.2.3	Tribulation calcite vein	168
6.2.4	Gilded Rose breccia type area	168
6.2.5	Mt Avarice quarry	169
6.2.6	Correlation of metasomatic assemblages	170
6.2.7	Spatial distribution of metasomatic assemblages	171
6.3	ISOTOPE GEOCHEMISTRY	171
6.3.1	$\delta^{18}\text{O}$ vs. $\delta^{18}\text{O}$ plots	174
6.3.2	$\delta^{18}\text{O}$ histograms	176
6.3.3	Summary	180
6.4	SILICATE CHEMISTRY	180
6.4.1	Feldspar chemistry	181
6.4.2	Clinopyroxene chemistry	181
6.4.3	Amphibole chemistry	183
6.4.4	Biotite Chemistry	187

6.5	OXIDE CHEMISTRY	193
6.5.1	Magnetite chemistry	194
6.5.2	Hematite chemistry	199
6.6	DISCUSSION	199
6.7	CONCLUSIONS	202

CHAPTER 7: 212
FLUID SOURCES AND FLUID-WALLROCK INTERACTION IN
REGIONAL ALTERATION AND IRON OXIDE-Cu-Au
MINERALISATION, EASTERN SUCCESSION, MT ISA BLOCK: INSIGHT
FROM C, O AND Sr ISOTOPES

7.1	INTRODUCTION	213
7.1.1	Regional Geology	214
7.1.2	Theoretical background, sampling and analytical procedures	217
7.2	CARBON and OXYGEN STABLE ISOTOPES	222
7.2.1	Mary Kathleen Fold Belt	222
7.2.2	Cloncurry District	226
7.2.3	Cloncurry District and Mary Kathleen Fold Belt comparisons	231
7.2.4	Zn-Pb-Ag mineralisation	236
7.2.5	Cu-Au mineralisation	238
7.3	STRONTIUM ISOTOPES	244
7.4	CATHODOLUMINESCENCE AND CARBONATE CHEMISTRY	245
7.4.1	Marbles	248
7.4.2	High temperature, sodic-(calcic) alteration systems	253
7.4.3	Retrograde breccias and veins	253
7.4.4	Ernest Henry ore breccia	256
7.4.5	Ernest Henry marble matrix breccia	256
7.5	DISCUSSION	258
7.5.1	Fluid pathways inferred from stable isotope ratios	258
7.5.2	Metasomatic fluid sources	260
7.5.3	Role of fluid-wallrock interaction in Cu-Au Mineralisation	263
7.6	CONCLUSIONS	265

CHAPTER 8:	273
SYNTHESIS AND CONCLUSIONS	
8.1 INTRODUCTION	274
8.2 STRUCTURAL FRAMEWORK	274
8.3 WIDESPREAD BRECCIATION IN THE CORELLA FORMATION	275
8.4 DILATIONAL FAULT ZONE CHARACTERISTICS	277
8.5 METASOMATIC FLUID SOURCES	279
8.6 METAL AND LIGAND SOURCES	281
8.7 STRUCTURAL AND GEOCHEMICAL SYNTHESIS	282
8.8 FE-OXIDE-CU-AU CLASSIFICATION	284
8.8.1 Mt Elliott-style deposits	284
8.8.2 Ernest Henry-style deposits	286
8.8.3 Reduced Cu-Au deposits	286
8.8.4 Starra-style deposits	287
8.8.5 Osborne-style deposits	287
8.9 SUMMARY	287
REFERENCES	289
APPENDICES	315
APPENDIX A: SAMPLE LIST	316
APPENDIX B: ISOTOPE DATA	321
APPENDIX C: MICROPROBE DATA	322
APPENDIX D: LA-ICPMS DATA	323

LIST OF FIGURES

CHAPTER 1

FIGURE 1.1.	3
Map of Precambrian Australia.	
FIGURE 1.2.	4
Tectonostratigraphic subdivisions of the Mt Isa Block.	
FIGURE 1.3.	5
Geology of the Eastern Succession, Mt Isa Block.	
FIGURE 1.4.	14
Eastern Succession geochronological ages.	
FIGURE 1.5.	15
Eastern Succession stratigraphic column.	
FIGURE 1.6.	21
Schematic E-W cross-section of the Eastern Succession.	

CHAPTER 2

FIGURE 2.1.	33
Geology of the Eastern Succession, Mt Isa Block.	
FIGURE 2.2.	37
TMI aeromagnetic structural skeleton map.	
FIGURE 2.3.	40
Aerial photograph with mapped geology from the Budenberri area.	
FIGURE 2.4.	41
Geological maps from the Tribulation and Mt Philp areas.	
FIGURE 2.5.	43
Geological map of the Cloncurry Region.	
FIGURE 2.6.	46
Structural geology map of the Spinifex area.	
FIGURE 2.7.	47
Block diagram of the Spinifex area.	

FIGURE 2.8.	49
Structural geology map of the Compass area.	
FIGURE 2.9.	50
Block diagram of the northern Compass area.	
FIGURE 2.10.	52
Block diagram of the northern Cloncurry District.	
FIGURE 2.11.	54
gOcad block diagram of upwards projected wavelet processed aeromagnetic data for the Cloncurry 1:100000 map sheet.	
FIGURE 2.12.	59
Schematic illustration of the effect of fault reactivation on fold geometry.	
FIGURE 2.13.	62
Model for the development of anomalous fold patterns in the northern Cloncurry District.	

CHAPTER 3

FIGURE 3.1.	68
Approximate fields for models for passive folding, flexural flow, TLS and TLS with the effects of a matrix with finite viscosity.	
FIGURE 3.2.	70
Profile sections of theoretical sinusoidal Class 1B folds and calculated strain ratio.	
FIGURE 3.3.	72
Examples of the propagation of fold related extensional fractures through competent layers.	
FIGURE 3.4.	74
Schematic representations of volume gain folding and effective layer thinning.	

CHAPTER 4

FIGURE 4.1.	79
Geology of the Eastern Succession, Mt Isa Block.	

FIGURE 4.2.	80
Geological map of the Cloncurry Region, highlighting the widespread distribution of brecciation.	
FIGURE 4.3.	82
Geometric fold classes and variables used in describing fold geometry.	
FIGURE 4.4.	84
Geometric boudin classification scheme.	
FIGURE 4.5.	87
Aerial photographs of D ₂ and D ₃ folds in the Soldier's Cap group.	
FIGURE 4.6.	89
Photographs and line drawings of D ₂ folds in the Corella Formation.	
FIGURE 4.7.	90
Outcrop map and photographs of pre-D ₃ boudins in the Corella Formation.	
FIGURE 4.8.	92
Aerial photographs and line drawings of D ₂ and D ₃ folds in the Corella Formation.	
FIGURE 4.9.	93
Photographs and line drawing of D ₃ folds in the Corella Formation.	
FIGURE 4.10.	95
Sketches from photographs of pre- and syn-D ₃ fracture geometries in the Corella Formation.	
FIGURE 4.11.	97
Photographs and sketches of complex geometries produced by folding of boudinaged and fractured sequences.	
FIGURE 4.12.	98
Photographs illustrating a continuum between fracturing, boudinage and brecciation processes in the Corella Formation.	
FIGURE 4.13.	100
Aerial photograph and mapped geology of D ₂ and D ₃ folds in the Budenberri Region.	
FIGURE 4.14.	102
Schematic illustration of the development of stratabound and discordant cataclastic breccias by boudin/clast rotation.	

FIGURE 4.15.	104
Illustration of the minimum amount of incompetent material required to accommodate space problems associated with Class 1b folding.	
 CHAPTER 5	
FIGURE 5.1.	116
Geology of the Eastern Succession, Mt Isa Block.	
FIGURE 5.2.	118
Illustration of the control of fault mode on the geometry of dilational zones and resultant fluid pressure gradients.	
FIGURE 5.3.	122
Simplified N-S cross section through the Mt Elliott Cu-Au deposit.	
FIGURE 5.4.	124
Photographs of Mt Elliott outer carapace breccias.	
FIGURE 5.5.	125
Outcrop map from the Roxmere waterhole.	
FIGURE 5.6.	127
Photographs of breccias and veins from the Roxmere – Marimo area.	
FIGURE 5.7.	128
Geological maps and sketch from a photograph from the Tribulation - Lime Creek area.	
FIGURE 5.8.	130
Photographs of breccias and veins from the Tribulation Quarry.	
FIGURE 5.9.	132
Geological map and sketches from photographs from the Gilded Rose breccia type area.	
FIGURE 5.10.	134
Photographs of breccias and granitic textures from within occurrences of Gilded Rose style brecciation.	
FIGURE 5.11.	136
Simplified cross-section through the Ernest Henry deposit.	

FIGURE 5.12.	137
Photographs of ore breccias and the marble matrix breccia from the Ernest Henry deposit.	
FIGURE 5.13.	139
Summary diagram of key features from Mt Elliott, Roxmere - Marimo, Tribulation, Gilded Rose and Ernest Henry.	
FIGURE 5.14.	141
Schematic fluid pressure curves for implosion brecciation.	
FIGURE 5.15.	143
Schematic pressure-time diagram, Mohr circles and cross-sections for the genesis of large width veins.	
FIGURE 5.16.	149
Schematic fluid pressure curves for fluidization and gas streaming.	
 CHAPTER 6	
FIGURE 6.1.	157
Geology of the Eastern Succession, Mt Isa Block.	
FIGURE 6.2.	160
Photographs of metasomatic rocks from the Roxmere – Marimo area, the Budenberri Rockhole, the Tribulation Quarry, the Gilded Rose type area, Camel Hill and the Mt Avarice Quarry.	
FIGURE 6.3.	163
Photomicrographs of typical metasomatic assemblages from the Roxmere – Marimo area, the Budenberri Rockhole, the Tribulation Quarry, Gilded Rose style breccias and the Mt Avarice Quarry.	
FIGURE 6.4.	166
Paragenetic diagrams for key field areas.	
FIGURE 6.5.	172
Alteration distribution maps for the Cloncurry Region.	
FIGURE 6.6.	175
$\delta^{18}\text{O}$ vs. $\delta^{18}\text{O}$ plots for metasomatic mineral pairs.	
FIGURE 6.7.	177
$\delta^{18}\text{O}$ fractionation curves for quartz, magnetite and actinolite.	

FIGURE 6.8.	178
Cumulative $\delta^{18}\text{O}$ histograms for silicate and oxide minerals in igneous rocks, regional alteration, and Cu-Au ore-proximal metasomatism.	
FIGURE 6.9.	182
Ternary plots for feldspar and pyroxene compositions.	
FIGURE 6.10.	184
Classification of calcic amphiboles.	
FIGURE 6.11.	185
Compositional fields for amphibole analyses.	
FIGURE 6.12.	188
Compositional fields for biotite analyses.	
FIGURE 6.13.	190
Plots of biotite-chlorine chemistry.	
FIGURE 6.14.	196
Trace element composition of magnetite grains.	
 CHAPTER 7	
FIGURE 7.1.	215
Geology of the Eastern Succession, Mt Isa Block.	
FIGURE 7.2.	218
Photographs of representative carbon and oxygen isotope samples.	
FIGURE 7.3.	223
Carbon and oxygen isotope data from MKFB marbles and calc-silicate rocks metasomatised during emplacement of the Burstall granite.	
FIGURE 7.4.	225
Carbon and oxygen isotope data from late to post-peak metamorphic metasomatic systems in the MKFB.	
FIGURE 7.5.	227
Carbon and oxygen isotope data from the Cloncurry District.	
FIGURE 7.6.	230
Carbon and oxygen isotope data from calcareous and carbonaceous lithologies, and breccia and vein infill within the Soldiers Cap Group of the Cloncurry District.	

FIGURE 7.7.	232
Carbon and oxygen isotope data from the Cloncurry District and MKFB.	
FIGURE 7.8.	235
Model curves for the depletion in carbon isotope values during metamorphic decarbonation.	
FIGURE 7.9.	237
Isotopic data from the Dugald River Zn-Pb-Ag deposit.	
FIGURE 7.10.	239
Carbon and oxygen isotopic data from the Ernest Henry deposit.	
FIGURE 7.11.	241
Isotope data from the Great Australia Cu-Au deposit.	
FIGURE 7.12.	242
Carbon and oxygen stable isotope data from Cu-Au deposits hosted within Cover Sequence 3.	
FIGURE 7.13.	246
Correlation diagram of $^{87}\text{Sr}/^{86}\text{Sr}$ vs. $1/\text{Sr}$ for Cloncurry District calcite samples.	
FIGURE 7.14.	247
$^{87}\text{Sr}/^{86}\text{Sr}$ vs. $\delta^{18}\text{O}$ ratios for Cloncurry District calcite samples.	
FIGURE 7.15.	249
CL images of textures commonly observed in Eastern Succession calcite grains.	
FIGURE 7.16.	252
Ternary diagrams of carbonate compositions.	
FIGURE 7.17.	254
CL images and associated microprobe traverse from Cloncurry District marbles.	
FIGURE 7.18.	255
CL images and microprobe traverses for calcite infill in sodic-(calcic) and retrograde breccias.	
FIGURE 7.19.	257
CL images and microprobe traverses for calcite in Ernest Henry ore breccia and marble matrix breccia.	
FIGURE 7.20.	259
Carbon and oxygen stable isotope data from Cloncurry District marbles, the Ernest Henry marble matrix breccia and sodic-(calcic) alteration.	

FIGURE 7.21. 264
Carbon and oxygen isotope data for all samples presented in this study.

CHAPTER 8

FIGURE 8.1. 278
Schematic cross-section of widespread brecciation within the Corella Formation,
and influence on fluid pressure.

FIGURE 8.2. 285
Schematic cross section of the Cloncurry District, illustrating the structural and
stratigraphic setting of various styles of late metamorphic Cu-Au mineralisation,
relative to brecciation in the Corella Formation.

LIST OF TABLES

CHAPTER 6

TABLE 6.1.	204
Data sources	
TABLE 6.2.	205
Mineral separate stable isotope data	
TABLE 6.3.	
Representative microprobe analyses	
6.3a. Feldspar	206
6.3b. Pyroxene	207
6.3c. Amphibole	208
6.3d. Biotite	209
TABLE 6.4.	210
Biotite-Cl chemistry	
TABLE 6.5.	211
Average magnetite mineral chemistry	

CHAPTER 7

TABLE 7.1.	267
MKFB carbon and oxygen isotope data from carbonates	
TABLE 7.2.	268
Cloncurry District carbon and oxygen isotope data from carbonates	
TABLE 7.3.	270
Ore deposit carbon and oxygen stable isotope data from carbonates	
TABLE 7.4.	272
Strontium isotope data from carbonates	